Echoes from classical black holes

Hyat Huang,[1] Min-Yan Ou,[1] Meng-Yun Lai,[1,*] and H. Lü[2]
[1]*College of Physics and Communication Electronics, Jiangxi Normal University, Nanchang 330022, China*
[2]*Center for Joint Quantum Studies and Department of Physics, School of Science, Tianjin University, Tianjin 300350, China*

(Received 10 January 2022; accepted 4 May 2022; published 24 May 2022)

We study echoes of free massless scalar from dyonic black holes in Einstein-Maxwell gravity extended with the quasitopological electromagnetic term. These asymptotically flat black holes all satisfy the dominant energy condition. We find that for suitable parameters, the effective potential can have double peaks and consequently echoes of quasinormal modes arise. In general the echo frequency associated with the initial wave packet released inside the two peaks is about twice the frequency of the one released outside.

DOI: 10.1103/PhysRevD.105.104049

I. INTRODUCTION

The discovery of gravitational waves (GWs) has launched an extraordinary new era in black hole physics. For the merging of two massive objects, the signals of late-time ringdowns encrypt important information that is worth studying. After the initial wave burst of the perturbation, the ringdown enters the stage of quasinormal modes (QNMs) that no longer depend on the initial disturbance; instead, they reflect the properties of the spacetime geometry. Therefore, it appears that QNMs are the best to study the black hole geometry that is characterized by having an event horizon. However, it was shown in Ref. [1] that QNMs are in fact related to the light rings of the massive objects, which are not necessarily black holes. It is therefore hard to distinguish black holes from other horizonless massive objects simply by studying their QNMs [2–4]. In fact, there are many exotic compact objects that can mimic the black holes, such as wormholes [5–8], boson stars [9–11], and firewalls [12,13].

Data analysis suggests that the recent Laser Interferometer Gravitational Wave Observatory observation appears to have detected the "echo" signals in the binary black hole waveforms [14,15]. The subject however remains controversial since opposite claims have also been put forward. In particular, Ref. [16] finds no evidence for echoes in many tests done by the LIGO-Virgo-KAGRA Collaboration (LVKC) using the third Gravitational-Wave Transient Catalog (GWTC-3). On the other hand, a recent study claims a putative "measurement" in GW190521[17]. These controversies have been inspiring theoretical exploration of the subject. However, the immediate study of QNMs in classical black holes indicates that it is hard to create such signals. It was suggested in [1,18,19] that echo signals could be used to distinguish the source of gravitational waves, whether it is from a black hole or not. Indeed, recent research in the perturbations of massive objects showed that echo signals could easily arise in phantom wormholes [20–24]. In fact, echoes can also come from other compact objects [25], and diverse sources including quark stars [26], braneworld black holes [27], neutron-star binary coalescences[28], ultracompact exotic stars[29], and even from a singularity [30]. However, it is hard to create echoes from the known traditional classical black hole geometries in Einstein gravity.

Whether black holes can have echoes thus becomes an important subject to study. Many ideas were put forward to create black hole echoes. Notable examples include quantum black holes [31–34], black hole with discontinuous effective potential [35], or with local Lorentz symmetry violations [36]. However, there is hitherto no example of classical black holes that can produce echoes. By "classical black holes," we refer to those constructed in Einstein gravity with minimally coupled matter. Of course, one can always write black hole metrics with desired properties. The difficulty is that we should require they satisfy some proper energy conditions, such as the dominant

*Corresponding author.
mengyunlai@jxnu.edu.cn

energy condition (DEC), or at least the weak energy condition (WEC).

In this paper, we draw the inspiration from the observation of the relation between the QNMs and the light rings, or photon spheres, for spherically symmetric configurations. In order to produce echoes, the effective potential should have double peaks so that signals can resonate between the peaks. This feature appears to be closely related to black holes with multiple-photon spheres. Such black holes indeed exist in Einstein-Maxwell gravity extended with quasitopological terms constructed from the Maxwell field strength [37,38]. The black holes all satisfy DEC, but can violate the strong energy condition (SEC). The violation of SEC relaxes the condition that gravity must be attractive, and consequently a stable photon sphere can exist, sandwiched between two unstable ones [37]. We find, as expected, that echoes can indeed emerge from these classical black holes.

In this paper, we study the free massless scalar perturbation, since we would like to use it to probe the spacetime geometry. The scalar does not interact directly with the Maxwell field, which for our purpose here merely provides the proper energy momentum tensor to support the black hole. As was suggested in [23,35], we can study such scalar perturbation as a proxy for gravitational perturbation. The echoes of scalar and electromagnetic perturbations from wormholes and braneworld black holes were investigated in Refs. [23,39].

The paper is organized as follows. In Sec. II, we give a general setup for the massless scalar perturbation and the numerical procedure. In Sec. III, we review the black holes constructed from the quasitopological electromagnetism and analyze the effective potentials of the scalar wave equation. In Sec. IV, we give our main results of QNMs that describe black hole echoes. We conclude the paper in Sec. V. In the Appendix, we compile various plots of our numerical results.

II. THE GENERAL SETUP

A. Massless scalar and the effective potential

In this paper, we consider only the static and spherically symmetric black holes, whose most general metric takes the form

$$ds^2 = -h(r)dt^2 + \frac{dr^2}{f(r)} + r^2 d\Omega_2^2. \tag{1}$$

We assume that the outer horizon of the black hole is located at r_+, with $h(r_+) = f(r_+) = 0$. To study the black hole echoes due to the metric only, we consider the free massless scalar perturbation, whose equation is

$$\Box\psi \equiv \frac{1}{\sqrt{-g}}\partial_\mu(\sqrt{-g}g^{\mu\nu}\partial_\nu\psi(t,r,\theta,\phi)) = 0. \tag{2}$$

For the background metric (1), the equation can be solved straightforwardly using the separation of variables:

$$\psi(t,t,\theta,\phi) = \Sigma_{l,m}\frac{\Phi(t,r)}{r}Y_{l,m}(\theta,\phi), \tag{3}$$

where $Y_{l,m}$ is the spherical harmonics. Under this, the scalar equation (2) reduces to

$$-\frac{\partial^2\Phi(t,r)}{\partial t^2} + hf\frac{\partial^2\Phi(t,r)}{\partial r^2} + \frac{1}{2}(fh' + hf')\frac{\partial\Phi(t,r)}{\partial r} - \left(\frac{l(l+1)}{r^2}h + \frac{1}{2r}(hf)'\right)\Phi(t,r) = 0, \tag{4}$$

where a prime denotes a derivative with respect to r. The radial coordinate r lies in the region $(r_+, +\infty)$. For QNMs, ingoing and outgoing boundary conditions should be, respectively, imposed on the horizon r_+ and at the asymptotical infinity. Therefore, QNMs do not probe the spacetime geometry inside the event horizon. It is instructive to use the tortoise coordinate to map the radial region to $(-\infty, \infty)$. Specifically, we define the tortoise radial coordinate r_* by

$$dr_* = \frac{dr}{\sqrt{hf}}. \tag{5}$$

Equation (4) can be cast as

$$-\frac{\partial^2\Phi}{\partial t^2} + \frac{\partial^2\Phi}{\partial r_*^2} - V(r)\Phi = 0, \tag{6}$$

where the effective potential V is given by

$$V(r) = \frac{l(l+1)}{r^2}h + \frac{1}{2r}(hf)'. \tag{7}$$

It is clear that after imposing the boundary condition, the property of the function Φ is solely determined by the effective potential V. It is worth noting that the tortoise coordinate transformation can stretch the potential but it does not change its shape, characterized by the number of extrema.

It can be easily seen that we have $V(r_+) = 0$ and $V'(r_+) > 0$. Furthermore at asymptotical infinity, we have $V(\infty) \to 0^+$ and $V'(\infty) \to 0^-$, assuming that $h \sim f \sim 1 - 2M/r + \cdots$, where M is the mass of the black hole. It follows that the potential $V(r)$ must have at least one maximum. In principle there can exist multiple peaks, with an odd number of total extrema. In typical black holes, including the Schwarzschild and the Reissner-Nordstrøm (RN) black holes, $V(r)$ has one extremum, which is the maximum, in which case we do not expect to have any echoes, since there is no mechanism for resonance. In order

to have echoes, we must have at least three extrema, with a minimum sandwiched between the two maxima. Such configurations of the effective potential arise naturally for wormholes, but are hard to come by in the case of black holes. It is thus natural to explore the conditions for which the potential (7) has at least double peaks.

One clue is provided by the observation that for large l, the leading term of the effective potential is dominant, i.e., $V \sim h/r^2$, which is precisely the effective potential for determining the photon spheres. The extrema of h/r^2 with positive h give the radii of the photon spheres, in the static and spherically symmetric spacetimes. The existence of multiple peaks of our effective potential is then closely related to the existence of multiple-photon spheres. Classical black holes with multiple-photon spheres are rare, but they do exist and we shall discuss them in Sec. III.

B. Numerical method

In this paper, we would like to solve wave equation (6) with the effective potential (7) and obtain the time-domain profile of $\Phi(r,t)$. We adopt the finite-difference method, which is effective in dealing with the QNMs of both black holes [40] and wormholes [23].

To obtain the finite-difference equation, we discretize the coordinates $t = i\Delta t$ and $r_* = j\Delta r_*$, where the i and j are integers. The scalar field Φ and the effective potential V are also discretized:

$$\Phi(t,r) = \Phi_{i,j} \equiv (i\Delta t, j\Delta r_*), \quad V(r_*) = V_j \equiv V(j\Delta r_*). \tag{8}$$

With this, the differential equation (6) becomes a set of iterative algebraic equations:

$$\begin{aligned} &-\frac{\Phi(i+1,j)-2\Phi(i,j)+\Phi(i-1,j)}{\Delta t^2} \\ &+\frac{\Phi(i,j+1)-2\Phi(i,j)+\Phi(i,j-1)}{\Delta r_*^2} \\ &-V(j)\Phi(i,j)=0. \end{aligned} \tag{9}$$

The above equation can be rewritten as

$$\begin{aligned} \Phi(i+1,j) = &-\Phi(i-1,j)+\left(2-2\frac{\Delta t^2}{\Delta r_*^2}-\Delta t^2 V(j)\right) \\ &\times\Phi(i,j)+\frac{\Delta t^2}{\Delta r_*^2}(\Phi(i,j+1)+\Phi(i,j-1)). \end{aligned} \tag{10}$$

For the time-domain profile, we adopt the corresponding standard outgoing (ingoing) boundary conditions,

$$\partial_t \Phi = \mp \partial_{r_*}\Phi, \quad \text{for } r_* \to \pm\infty, \tag{11}$$

and follow Ref. [41] to implement the codes. It should be pointed out that in our numerical calculation using the time-domain finite-difference method, the boundary condition is actually inessential as long as the signals do not reach the bound of the grids, as observed in Ref. [35]. According to the von Neumann stability condition, we set $\Delta t/\Delta r_* = 0.5$ in our numerical calculations. More details are referred to Ref. [40]. Our goal is to solve the above equations, starting from a certain initial wave packet. For convenience, we set it in Gaussian distribution, i.e.,

$$\psi(t=0,r_*) = e^{-\frac{(r_*-\bar{a})^2}{2}}, \quad \text{and} \quad \psi(t<0,r_*) = 0. \tag{12}$$

The parameter $\bar{a}$ is the location of the center of the initial wave packet. Two inequivalent situations can be considered. One is that the wave packet is outside the double peaks. In this case we find the echoing QNMs have the same characteristics whether it is put close to the horizon or out away from the peaks. We therefore present the results only for the latter case. Another intriguing situation is when we put the initial wave packet in the potential well between the two peaks. We find when the releasing location $\bar{a}$ is closer to the bottom of the potential well, the echo signals will become more distinguishable. Furthermore, the echo frequency, or the number of echoes, roughly doubles the one associated with the wave packet outside the peaks.

III. BLACK HOLES AND DOUBLE-PEAK POTENTIALS

A. Black holes from quasitopological electromagnetism

In this section, we review Einstein-Maxwell gravity extended with a quartic-order quasitopological term constructed from the Maxwell field strength $F = dA$. The Lagrangian is [37]

$$\mathcal{L} = \sqrt{-g}(R - F^{\mu\nu}F_{\mu\nu} - \alpha((F^{\mu\nu}F_{\mu\nu})^2 - 2F^{\mu}_{\nu}F^{\nu}_{\rho}F^{\rho}_{\sigma}F^{\sigma}_{\mu})), \tag{13}$$

where α is the coupling constant of the quasitopological term. The theory admits an exact solution of asymptotically flat dyonic black holes that are both static and spherically symmetric:

$$\begin{aligned} ds^2 &= -h dt^2 + \frac{dr^2}{h} + r^2(d\theta^2 + \sin^2\theta d\varphi^2), \\ F &= -\frac{qr^2}{r^4+4\alpha p^2} dt \wedge dr + p\sin\theta d\theta \wedge d\varphi, \end{aligned} \tag{14}$$

with

$$h = 1 - \frac{2M}{r} + \frac{p^2}{r^2} + \frac{q^2}{r^2}\,{}_2F_1\left(\frac{1}{4},1;\frac{5}{4};-\frac{4\alpha p^2}{r^4}\right). \tag{15}$$

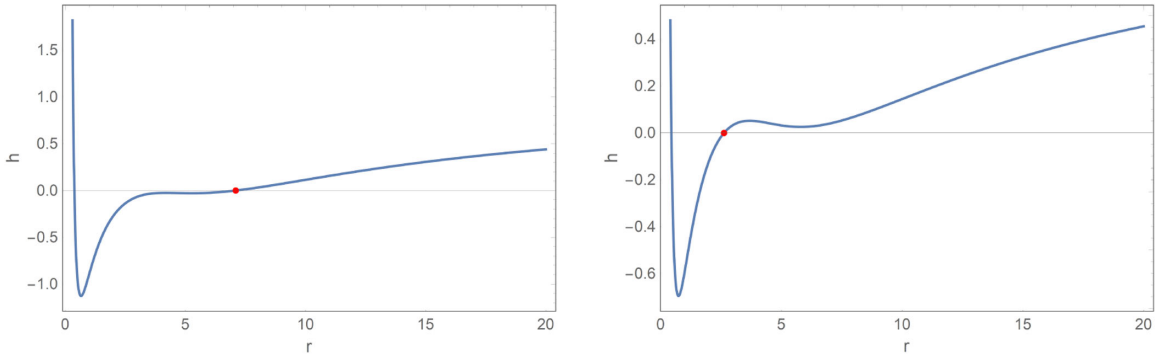

(a) $M = 6.80$ (b) $M = 6.65$

FIG. 1. Here, we give the metric profile function $h(r)$ for two different masses, with $(\alpha, p, q) = (149.90, 0.945, 6.863)$. Both black holes have two horizons, but depending on the mass, we see that the function h may not be monotonous outside the outer horizon, indicated by the red dot.

The general solution contains three integration constants: the mass M, and the electric and magnetic charges (q, p). When $\alpha qp = 0$, the solution reduces to the usual RN black hole. The properties of these black holes were analyzed in [37]. They all satisfy DEC, but can violate SEC. For suitable parameters, black holes with four horizons can emerge. In this paper, we are interested in black holes with two horizons, but with an unusual feature that the profile function h is not monotonous outside the horizon. It has an extra wiggle such that the gravity force can vanish and even be repulsive in a certain finite region outside the horizon. This feature is a direct consequence of the SEC violation.

For a concrete example, we choose the parameters, e.g., $(\alpha, p, q) = (149.90, 0.945, 6.863)$. For $M < 6.370$, solution is overcharged and the curvature singularity at $r = 0$ is naked. When $6.355 < M < 6.729$, the black hole has two horizons and h is not monotonous outside the outer horizon, but has a wiggle with a local maximum and a minimum. Further increasing the mass such that $6.723 < M < 6.760$, the local minimum dips down to be negative so that the black hole has four horizons. When $M > 6.760$, the two inner horizons disappear and the black hole reverts back to having two horizons.[1] In the last two cases, the function h is monotonous outside the outer horizon. In Fig. 1, we present the plots for the function h for $M = 6.80$ and $M = 6.65$.

We see from Fig. 1 that both black holes with $M = 6.80$ and $M = 6.65$ have two horizons. However, when $M = 6.80$, the function h is monotonous outside the horizon, but it has a wiggle when $M = 6.65$. This extra wiggle implies that the black hole has three photon spheres, with a stable photon sphere sandwiched between two unstable ones [37]. As we have discussed earlier, we expect that such spacetime geometry will give rise to the effective potential with double peaks, which we discuss in the next subsection.

B. Effective potentials of black hole solutions

The effective potential of the massless scalar wave is given by (7). For our case, we have $f = h$, with h given by (15). We find that there are two types of effective potentials, depending on the values of the black hole parameters. One involves a single peak, and the other has double peaks. Taking the same values associated with Fig. 1, we present the corresponding effective potentials using the tortoise coordinates in Fig. 2.

We see from Fig. 2 that when $M = 6.80$, the effective potential has a single peak, which is typical for many black holes including the Schwarzschild and RN black holes. It has been pointed out in Ref. [36] that such black holes cannot produce echoes, without introducing a reflective boundary condition by hand.

Producing echoes in classical black holes calls for effective potentials with at least two peaks. They are easy to realize in wormhole metrics [20,21,23,24]. However, there are few such black holes. For the $M = 6.65$ black hole, the double-peak potential is achieved by violating SEC such that gravity can be repulsive in certain regions of spacetime. However, since our solutions satisfy DEC, they can nevertheless be models for realistic black holes. It is worth remarking that the integration constant of the tortoise coordinate r_* does not affect the shape of the potential, but it provides a constant shift. We have fixed the constant such that the single or double peaks of the potential are located in the vicinity at $r_* = 0$, as shown in Fig. 2.

[1]Note that the black hole metric (14) is invariant under the constant scaling $(t, r, M, p, q, \alpha) \to (\lambda t, \lambda r, \lambda M, \lambda p, \lambda q, \lambda^2 \alpha)$, up to an overall conformal factor λ^2 to the metric. It is thus useful to convert to dimensionless parameters $(M^*, p^*, q^*) = (M, p, q)/\sqrt{\alpha}$ to distinguish different solutions. These dimensionless parameters correspond effectively to setting $\alpha = 1$.

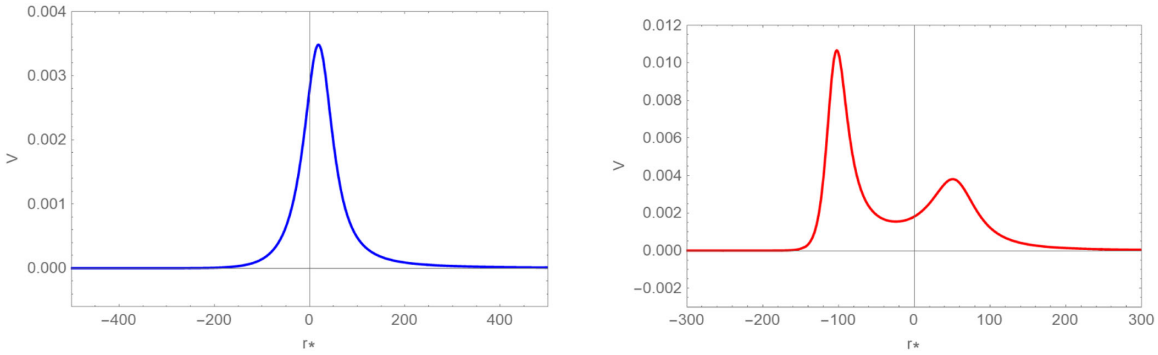

(a) Potential with single peak at $M = 6.80$ (b) Potential with double peaks at $M = 6.65$

FIG. 2. Two typical shapes of the effective potentials are plotted in terms of the tortoise coordinates. The parameters here are chosen to be $\alpha = 149.90$, $p = 0.945$, $q = 6.863$, and $l = 1$.

Having established that the double-peak potential can arise, we explore the parameter space around the above example to see how the potential depends on various parameters including the mass, charge, and also the l parameter associated with the spherical harmonics. In order not to interrupt the flow of the main text, we present all the plots of the double-peak potentials in the Appendix. The effective potential depends on (M, q, p, l, α). In Figs. 5, 7, and 9 in the Appendix, we give the effective potentials with varying M, q, and l, respectively. It should be mentioned that when $l \neq 0$, the effective potential is always non-negative. However, when $l = 0$, there may exist regions where the potential becomes negative. We find that in this case the echoes are not discernible. In the next subsection, we study the time-domain profiles of the corresponding QNMs and see that they generally produce echoes.

While the existence of multiple-photon spheres provides the inspiration for double-peak potentials when the first term in (7) is dominant, the second term in (7) suggests that echoes may happen even when the function h is monotonous, provided that h' is not. We shall present such an example in the next section, together with its echoing QNM.

IV. NUMERICAL ECHOES FROM BLACK HOLES

In this section, we present our main results, namely the QNMs that carry the echo signals when the effective potentials have double peaks. As we mentioned in the setup, there are two situations to consider: (1) the initial wave packet is outside the two peaks; (2) it is between the two peaks.

A. Wave packet outside the double peaks

Here, we present the results for the first case. For the purpose of comparison, we first give the QNM when the potential has only one peak. We consider the $M = 6.80$ case of Figs. 1 and 2. As expected, the original wave packet evolves as a damping oscillator, and it produces no echoes, as can be seen by the left column of Fig. 3.

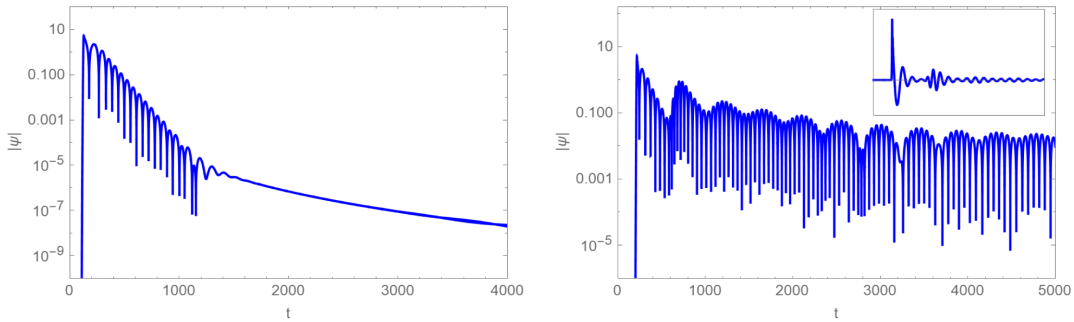

(a) No echoes from single-peak potential (b) Echoes from double-peak potential

FIG. 3. These two time-domain profiles correspond to the effective potentials shown in Fig. 2, where we set $\alpha = 149.90$, $p = 0.945$, $q = 6.863$, $l = 1$. The left column has $M = 6.8$ while the right column has $M = 6.65$. They show that there is no echo for the single-peak potential, while the echoes arise in double-peak potential.

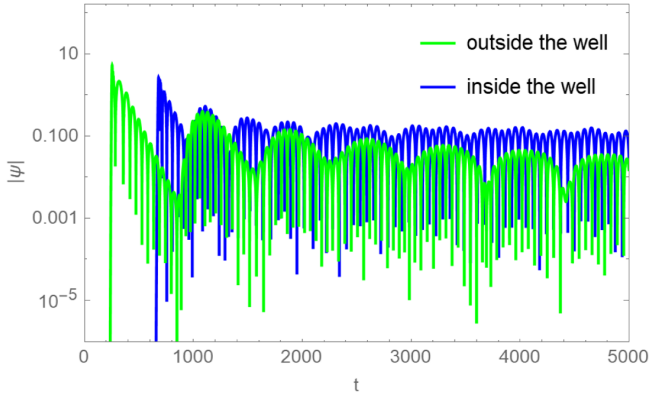

FIG. 4. Here are the time-domain profiles of initial wave packets released inside and outside the two potential peaks. The corresponding V is plotted in Fig. 5 in the Appendix with $\alpha = 149.90, p = 0.945, q = 6.86, l = 1, M = 6.7$. The green lines correspond to the initial wave packet at $r_* = 100$ (outside the well). The blue lines correspond to the initial wave packet at $r_* = -76$ (the bottom of the well). The echo frequency of the latter is about twice of the former, and the shapes are less pronounced.

For the double-peak potentials, we can observe the echo signals after the initial damping of the wave packet. A concrete example of the time-domain profile of the echoes is presented in the right column of Fig. 3. It is clear that the echoes arise because of resonant reflection by the two peaks. Therefore the frequency, or the number of echoes, does not depend on the releasing position, as long as they are outside the two peaks. (We shall study presently the case when the initial wave packet is released inside the two peaks.) It should also be noted that for the fixed parameters (α, p, q, l) given in Fig. 3, the black hole can echo when its mass lies within $6.51 < M < 6.73$. The $M = 6.65$ case is just one example presented. This illustrates that although there is only a small window of parameters under which the black hole echoes, the phenomenon is not a fine-tuned one.

As we discussed in the previous section, we have obtained many examples of double-peak potentials by varying parameters such as M, q, and l. We construct the corresponding QNMs and obtain the time-domain profiles. We present the results in the Appendix in Figs. 6, 8, and 10, respectively. As we can see, the signature of echo signals depends on many factors and to distinguish them requires precision measurements. One special case is worth mentioning, namely $l = 0$. The effective potential can be negative in some regions and the echo signals are hardly discernible. The existence of the negative region of effective potential raises the specter that the spacetime geometry may be unstable. However, our numerical analysis indicates that there is no unstable time-domain profile, which is consistent with the fact that in the region $M \in (6.355, 6.729)$ where the double peaks arise, we find that $\int_{-\infty}^{+\infty} V(r_*) dr_*$ is always positive.

From these examples, one might draw a conclusion that the double-peak potential arises only in the case when $h(r)$ is not monotonically increasing. However, this is not true. We find an example where $h(r)$ is in fact monotonically increasing outside the horizon, but the corresponding effective potential continues to have double peaks. This case arises when we choose the following parameters:

$$\alpha = 123.90, \qquad p = 1.181, \qquad q = 6.863,$$
$$l = 3, \qquad M = 6.58. \tag{16}$$

It is clear that the second term in (7) can also give nontrivial contribution since h' is not monotonous is this case. Our numerical study shows that this black hole can also produce echoes, although the signals are less clear in later time. We show the results of this example in Fig. 11 in the Appendix.

B. Wave packet within the double peaks

In the previous subsection, we focused on echoes of the initial wave packet released outside the two peaks of the effective potential. We now release it in the potential well between the two peaks. As a concrete example, we consider the potential given in Fig. 5 in the Appendix, with $\alpha = 149.90, p = 0.945, q = 6.863, l = 1, M = 6.7$. We find that the echo signals become more sensitive to the exact release location. In particular, the echoes become more distinguished when the releasing location is at the bottom of the potential well, in which case we find that the echo frequency nearly doubles. This phenomenon is explicitly depicted in Fig. 4, and we see that echoes of the wave packet outside the peak are much more pronounced. The physical process for this phenomenon can be explained as follows. The initial Gaussian packet moves both to the left and right at the same time, thereby effectively creating two packets that individually undergo a different number of reflections. Hence, the distance between the echoes depends on the initial location of the wave packet being inside or outside the two potential peaks. A similar mechanism was discussed in Ref. [42].[2]

V. CONCLUSION

In this paper, we studied the echoes of a free scalar wave packet initially released outside the dyonic black hole in Einstein-Maxwell gravity extended with quartic quasitopological terms constructed by the Maxwell field strength. We were motivated by the observation that the phenomenon of black hole echoes was closely related to having multiple-photon spheres. It was well established that these black holes could admit multiple-photon spheres, and not

[2]We are grateful to the referee for pointing this out.

surprisingly, our QNM constructions showed that they indeed could have echoes for suitable parameters. For the black hole considered, our numerical data indicate that the echoes occur within a small window of parameters, but the phenomenon is not a fine-tuned one. Intriguingly, we found that when the initial wave packet is released in the bottom of the potential well between the two peaks, its echo frequency is about doubled, compared to the case when the wave packet is released outside the two peaks. We expect that a similar phenomenon should occur in echoes from non-black hole objects, but it is certainly worth checking.

It should be emphasized that our results do not dispute the fact that the Schwarzschild or RN black holes do not have echoes within the framework of general relativity. In fact, the black holes of the quasitopological electromagnetism are not realistic in that they carry both electric and magnetic charges and our data analysis required a large coupling constant α. However, it is important to stress that these black holes all satisfy DEC, and that the free scalar probes only the geometry. In other words, the quasitopological electromagnetism plays no particular role other than providing the proper matter energy-momentum tensor to curve the spacetime. Our results therefore establish the general statement that traditional classical black holes in Einstein gravity coupled to suitable matter satisfying DEC can produce echoes. An observation of echoes in itself cannot rule out the black hole source, without precision measurements.

The connection between black hole echoes and multiple-photon spheres becomes apparent for large l; however, we found that echoes could also arise even when h is monotonous outside the event horizon, when the second term in the effective potential (7) becomes nontrivial. Therefore, it is far from clear what the necessary condition is for a black hole to echo. It is nevertheless tempting to conjecture that black holes satisfying SEC cannot produce echoes, or more weakly, the no-echo condition requires both SEC and DEC.

ACKNOWLEDGMENTS

We are grateful to Peng Liu, Senping Luo, Bing Sun, and Runqiu Yang for useful discussions. H. L. is supported in part by the National Natural Science Foundation of China (NSFC) Grants No. 11875200 and No. 11935009.

APPENDIX: PLOTS OF POTENTIALS AND ECHOING TIME-DOMAIN PROFILES

In this Appendix, we compile all the figures mentioned in the main text. For appropriately chosen parameters, we obtain the effective potential $V(r)$ in (7) with double peaks and we draw the corresponding echoing QNMs.

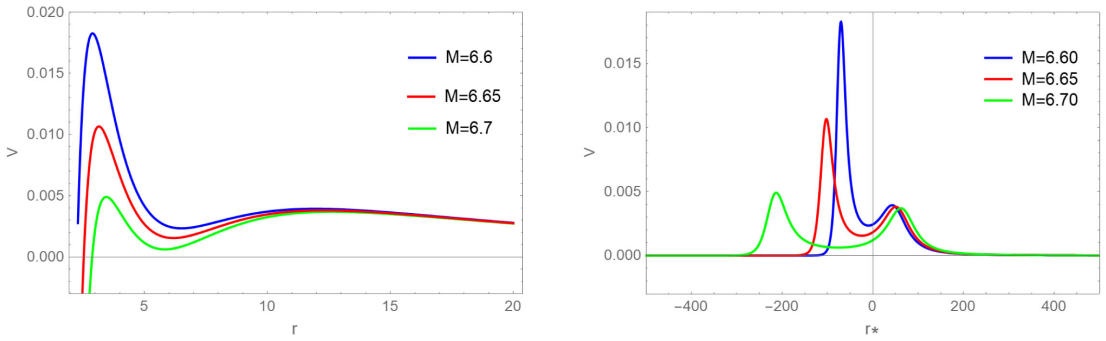

(a) $V(r)$ (b) $V(r_*)$

FIG. 5. Here, we fix the parameters $\alpha = 149.90$, $p = 0.945$, $q = 6.863$, $l = 1$ and vary the mass M. In the left, the potential is plotted as a function of r, and in the right as a function of r_*. The mass lies in a narrow region where V has two peaks. These potentials lead to echo signals presented in Fig. 6.

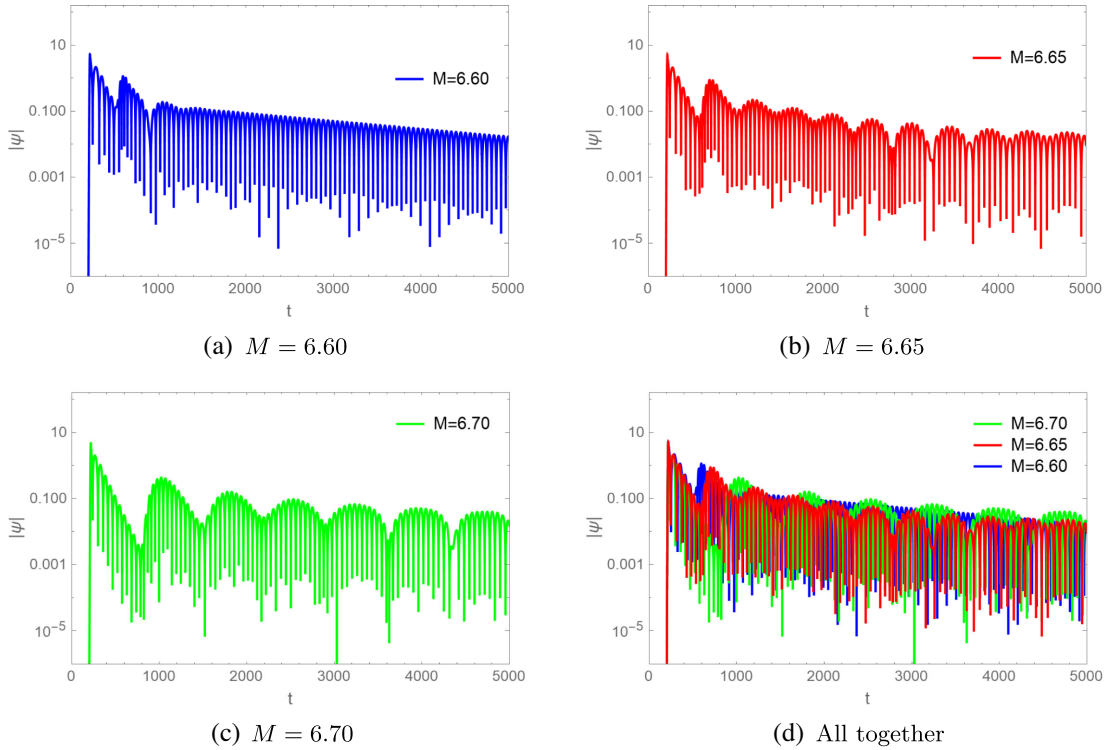

(a) $M = 6.60$ (b) $M = 6.65$

(c) $M = 6.70$ (d) All together

FIG. 6. These are the time-domain profiles with varying M, associated with the effective potentials given in Fig. 5. The echoes are more pronounced with larger mass in these parameters' regions.

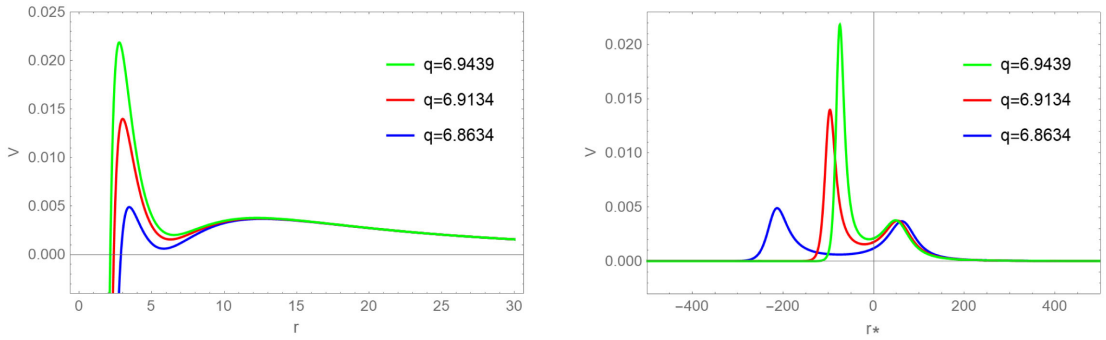

(a) $V(r)$ (b) $V(r_*)$

FIG. 7. In these plots, we fix $M = 6.7, \alpha = 149.90, p = 0.945, l = 1$ and study the effective potential by varying the electric charge q.

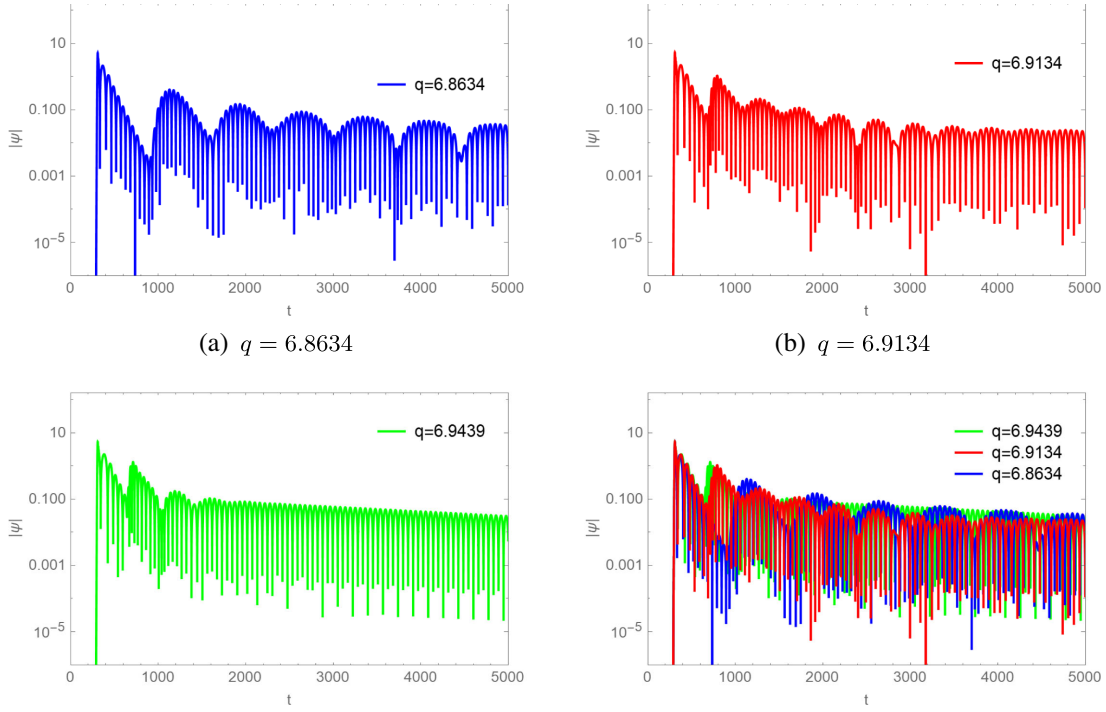

(a) $q = 6.8634$ (b) $q = 6.9134$

(c) $q = 6.9439$ (d) All together

FIG. 8. These are time-domain profiles with varying q, associated with the effective potentials given in Fig. 7. The echo is most pronounced for the smallest q in this set of parameters.

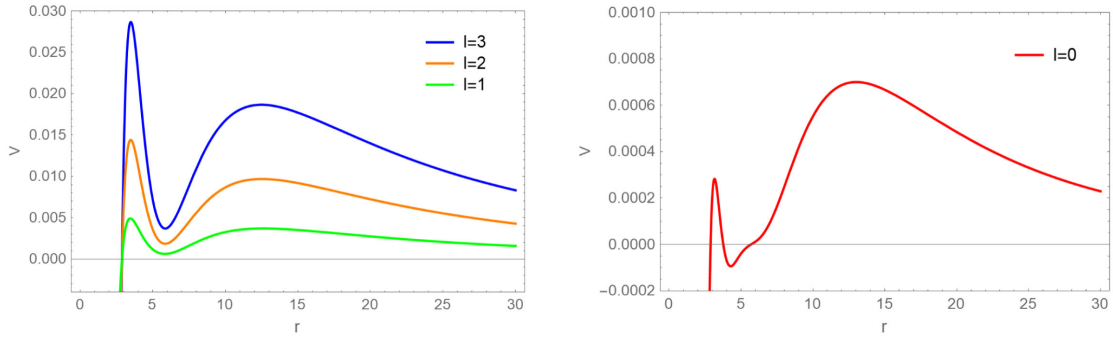

(a) $l \neq 0$ (b) $l = 0$

FIG. 9. Here we consider varying the parameter l, with fixed $M = 6.7, \alpha = 149.90, p = 0.945, q = 6.863$. The left shows V with $l \neq 0$; the right shows V with $l = 0$. Larger l causes higher peaks. When $l = 0$, the potential can be negative in some middle regions.

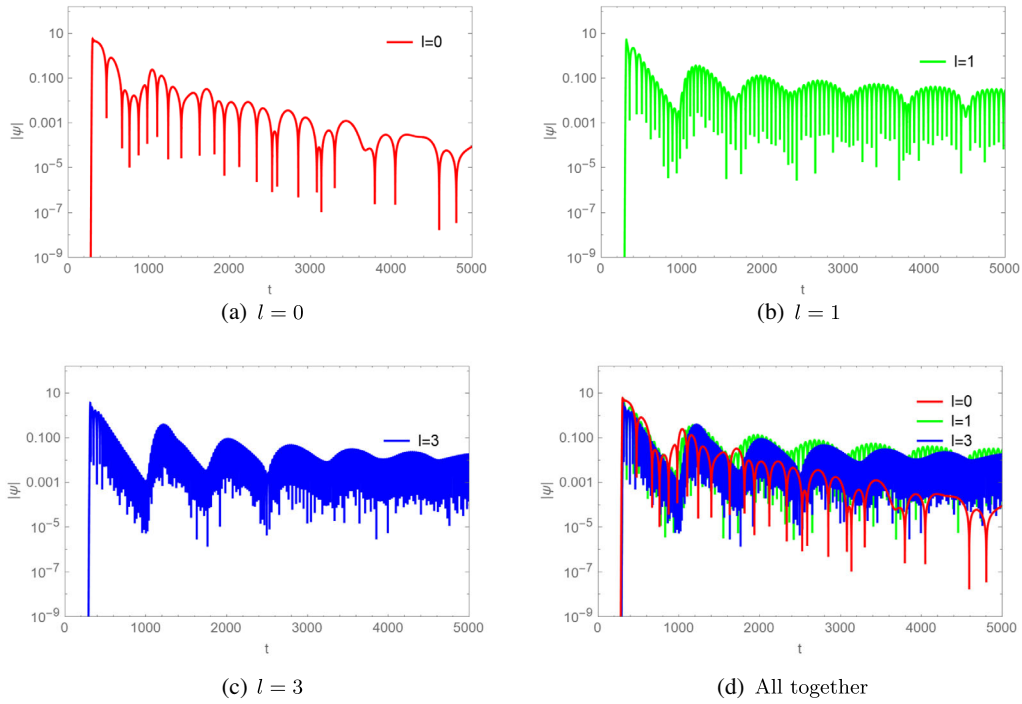

(a) $l = 0$ (b) $l = 1$

(c) $l = 3$ (d) All together

FIG. 10. Here are the time-domain profiles of varying l, associated with the double-peak potentials given in Fig. 9. When $l = 0$, the echo is hardly discernible, perhaps due to having a negative potential region.

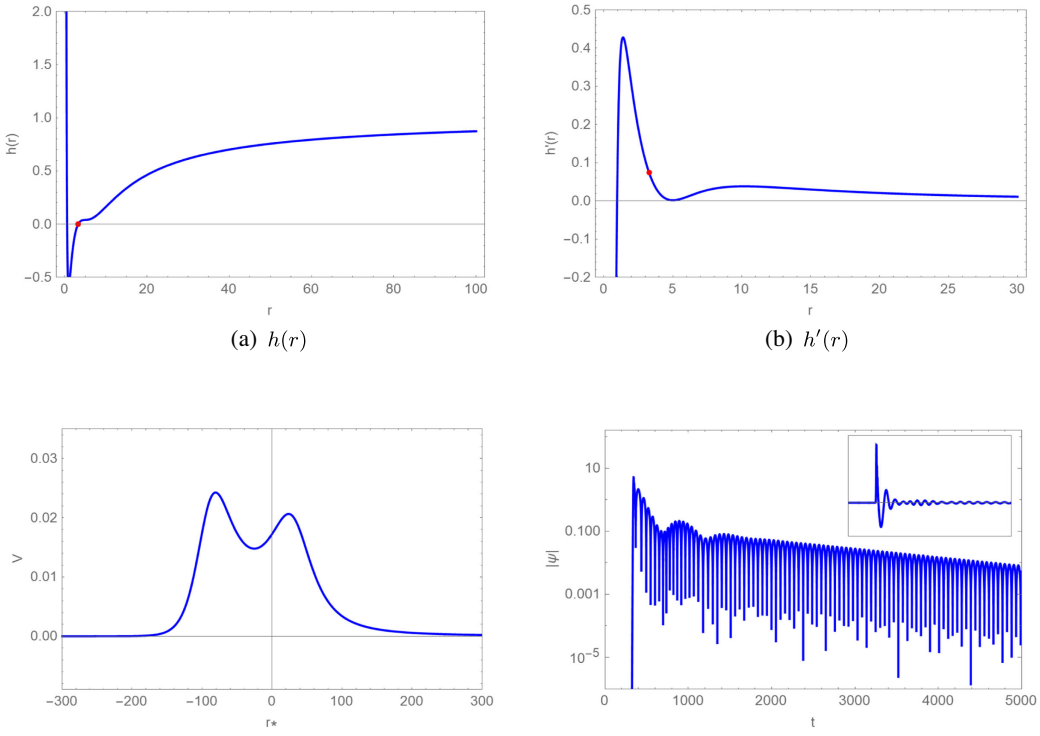

(a) $h(r)$ (b) $h'(r)$

(c) $V(r_*)$ (d) Echoes

FIG. 11. Here, we show that the double-peak potential can also arise even when the function h is monotonous outside the horizon, provided that h' is not. The black hole continues to satisfy DEC, but not SEC. The red point indicates the location of the outer horizon. This black hole can also produce echoes, although they become indiscernible in later time. Here, we set $\alpha = 123.90$, $p = 1.181$, $q = 6.863$, $l = 3$, $M = 6.58$.

[1] V. Cardoso, E. Franzin, and P. Pani, Is the Gravitational-Wave Ringdown a Probe of the Event Horizon?, Phys. Rev. Lett. **116**, 171101 (2016); **117**, 089902(E) (2016).

[2] E. Berti, V. Cardoso, and A. O. Starinets, Quasinormal modes of black holes and black branes, Classical Quantum Gravity **26**, 163001 (2009).

[3] Z. Mark, A. Zimmerman, S. M. Du, and Y. Chen, A recipe for echoes from exotic compact objects, Phys. Rev. D **96**, 084002 (2017).

[4] R. A. Konoplya and A. Zhidenko, Quasinormal modes of black holes: From astrophysics to string theory, Rev. Mod. Phys. **83**, 793 (2011).

[5] H. Huang and J. Yang, Charged Ellis wormhole and black bounce, Phys. Rev. D **100**, 124063 (2019).

[6] H. Huang, H. Lü, and J. Yang, Bronnikov-like wormholes in Einstein-scalar gravity, arXiv:2010.00197.

[7] P. Kanti, B. Kleihaus, and J. Kunz, Wormholes in Dilatonic Einstein-Gauss-Bonnet Theory, Phys. Rev. Lett. **107**, 271101 (2011).

[8] B. Kleihaus and J. Kunz, Rotating Ellis wormholes in four dimensions, Phys. Rev. D **90**, 121503 (2014).

[9] F. E. Schunck and E. W. Mielke, General relativistic boson stars, Classical Quantum Gravity **20**, R301 (2003).

[10] B. Kleihaus, J. Kunz, and M. List, Rotating boson stars and Q-balls, Phys. Rev. D **72**, 064002 (2005).

[11] B. Hartmann, B. Kleihaus, J. Kunz, and M. List, Rotating boson stars in 5 dimensions, Phys. Rev. D **82**, 084022 (2010).

[12] A. Almheiri, D. Marolf, J. Polchinski, and J. Sully, Black holes: Complementarity or firewalls?, J. High Energy Phys. 02 (2013) 062.

[13] D. E. Kaplan and S. Rajendran, Firewalls in general relativity, Phys. Rev. D **99**, 044033 (2019).

[14] J. Abedi, H. Dykaar, and N. Afshordi, Echoes from the Abyss: Tentative evidence for Planck-scale structure at black hole horizons, Phys. Rev. D **96**, 082004 (2017).

[15] J. Abedi, H. Dykaar, and N. Afshordi, Echoes from the Abyss: The holiday edition!, arXiv:1701.03485.

[16] R. Abbott *et al.* (LIGO Scientific, VIRGO, and KAGRA Collaborations), Tests of general relativity with GWTC-3, arXiv:2112.06861.

[17] J. Abedi, L. F. L. Micchi, and N. Afshordi, GW190521: First measurement of stimulated Hawking radiation from black holes, arXiv:2201.00047.

[18] V. Cardoso and P. Pani, Tests for the existence of black holes through gravitational wave echoes, Nat. Astron. **1**, 586 (2017).

[19] V. Cardoso, S. Hopper, C. F. B. Macedo, C. Palenzuela, and P. Pani, Gravitational-wave signatures of exotic compact objects and of quantum corrections at the horizon scale, Phys. Rev. D **94**, 084031 (2016).

[20] P. Bueno, P. A. Cano, F. Goelen, T. Hertog, and B. Vercnocke, Echoes of Kerr-like wormholes, Phys. Rev. D **97**, 024040 (2018).

[21] K. A. Bronnikov and R. A. Konoplya, Echoes in brane worlds: Ringing at a black hole–wormhole transition, Phys. Rev. D **101**, 064004 (2020).

[22] M. S. Churilova and Z. Stuchlik, Ringing of the regular black-hole/wormhole transition, Classical Quantum Gravity **37**, 075014 (2020).

[23] H. Liu, P. Liu, Y. Liu, B. Wang, and J. P. Wu, Echoes from phantom wormholes, Phys. Rev. D **103**, 024006 (2021).

[24] M. Y. Ou, M. Y. Lai, and H. Huang, Echoes from asymmetric wormholes and black bounce, arXiv:2111.13890.

[25] R. A. Konoplya, Z. Stuchlík, and A. Zhidenko, Echoes of compact objects: New physics near the surface and matter at a distance, Phys. Rev. D **99**, 024007 (2019).

[26] D. Kartini and A. Sulaksono, Gravitational wave echoes from quark stars, J. Phys. Conf. Ser. **1572**, 012034 (2020).

[27] R. Dey, S. Chakraborty, and N. Afshordi, Echoes from braneworld black holes, Phys. Rev. D **101**, 104014 (2020).

[28] P. Pani and V. Ferrari, On gravitational-wave echoes from neutron-star binary coalescences, Classical Quantum Gravity **35**, 15LT01 (2018).

[29] A. Urbano and H. Veermäe, On gravitational echoes from ultracompact exotic stars, J. Cosmol. Astropart. Phys. 04 (2019) 011.

[30] A. Chowdhury and N. Banerjee, Echoes from a singularity, Phys. Rev. D **102**, 124051 (2020).

[31] Q. Wang, N. Oshita, and N. Afshordi, Echoes from quantum black holes, Phys. Rev. D **101**, 024031 (2020).

[32] K. Saraswat and N. Afshordi, Quantum nature of black holes: Fast scrambling versus echoes, J. High Energy Phys. 04 (2020) 136.

[33] N. Oshita, D. Tsuna, and N. Afshordi, Quantum black hole seismology I: Echoes, ergospheres, and spectra, Phys. Rev. D **102**, 024045 (2020).

[34] S. K. Manikandan and K. Rajeev, New kind of echo from quantum black holes, Phys. Rev. D **105**, 064024 (2022).

[35] H. Liu, W. L. Qian, Y. Liu, J. P. Wu, B. Wang, and R. H. Yue, Alternative mechanism for black hole echoes, Phys. Rev. D **104**, 044012 (2021).

[36] G. D'Amico and N. Kaloper, Black hole echoes, Phys. Rev. D **102**, 044001 (2020).

[37] H. S. Liu, Z. F. Mai, Y. Z. Li, and H. Lü, Quasi-topological electromagnetism: Dark energy, dyonic black holes, stable photon spheres and hidden electromagnetic duality, Sci. China Phys. Mech. Astron. **63**, 240411 (2020).

[38] A. Cisterna, G. Giribet, J. Oliva, and K. Pallikaris, Quasi-topological electromagnetism and black holes, Phys. Rev. D **101**, 124041 (2020).

[39] R. Dey, S. Biswas, and S. Chakraborty, Ergoregion instability and echoes for braneworld black holes: Scalar, electromagnetic, and gravitational perturbations, Phys. Rev. D **103**, 084019 (2021).

[40] Z. Zhu, S. J. Zhang, C. E. Pellicer, B. Wang, and E. Abdalla, Stability of Reissner-Nordström black hole in de Sitter background under charged scalar perturbation, Phys. Rev. D **90**, 044042 (2014).

[41] J. O. Ruoff, The numerical evolution of neutron star oscillations, arXiv:gr-qc/0010041.

[42] E. Maggio, A. Testa, S. Bhagwat, and P. Pani, Analytical model for gravitational-wave echoes from spinning remnants, Phys. Rev. D **100**, 064056 (2019).